Fabrication and physical properties of self-organized silver nanocrystals*

M. P. Pileni

*Laboratoire SRSI, URACNRS 1662, Université P. et M. Curie (Paris VI), B.P. 52,
4 Place Jussieu, F - 752 31 Paris Cedex 05, France*

Abstract: A simple method is used to prepare highly monodispersed silver nanoparticles in the liquid phase, which starts from an initial synthesis in functionalized AOT reverse micelles. To narrow the particle size distribution from 43 to 12.5% in dispersion, the particles are extracted from the micellar solution. The size-selected precipitation method is used. The nanocrystallites dispersed in hexane are deposited on a support. A monolayer made of nanoparticles with spontaneous compact hexagonal organization is observed. The immersion of the support on the solution yields to the formation of organized multilayers arranged as microcrystal in a face-centered-cubic structure.

We compare the optical properties of spherical particles organized in a two- and three-dimensional structure with isolated and disordered particles. When particles, deposited on cleaved graphite, are arranged in a hexagonal array, the optical measurements under p-polarization show a new high-energy resonance, which is interpreted as a collective effect, resulting from optical anisotropy due to the mutual interactions between particles. We support this interpretation by numerical calculations performed for finite-size clusters of silver spheres. For disordered particles, a low-energy resonance appears instead of the high-energy resonance observed for spherical and organized particles. This is interpreted as optical shape anisotropy due to the asymmetrical arrangement of particles.

The tip of a scanning tunneling microscope (STM) may be used as an extremely localized source of low-energy electrons to locally excite photon emission from a variety of metal films. The detection of locally excited luminescence at the junction of an STM tip provides access to electron dynamic properties at the surface, which makes it possible to study luminescence phenomena of nanometer-sized structures.

The photon intensity emitted from electrically isolated silver nanoparticles self-organized as a 2D network on a gold (111) substrate is analyzed. We observed unexpectedly strong variations of photon-emission efficiency from isolated nanoparticles, depending on how tightly they are embedded within the network site. The quenching site observed in the STM photon emission map is interpreted as an enhanced interaction of electrons with surface photon modes.

INTRODUCTION

There is currently intense interest in examining the properties of nanosized metal particles, which differ greatly from those of bulk material. Nanostructures which include small-dimension systems and nanometer-sized clusters exhibit surprises and novel phenomena linked to nanometer dimensions. Well-ordered arrays of nanoparticles represent an exciting new class of materials, which provide opportunities for optimizing material properties and offer possibilities for probing a new and potential collective phenomenon. The development of the ultimate properties of these ordered nanostructures is the future

direction in metal science.

Such a class of materials has been produced by using different techniques [1–11], including reverse micelles [1–3]. Several years ago, by using this technique, silver nanoparticles with sizes varying from 2 to 8 nm [12] were prepared. To obtain a narrow size distribution of these particles, a size-selection precipitation method was used [13]. The selected particles deposited on cleaved graphite substrates were self-assembled either as a monolayer organized in a hexagonal network, or in three-dimensional (3D) superlattices with a face-centered-cubic (fcc) structure. Similar arrangements were obtained a few years ago with silver sulfide nanoparticles [14–16]. By using different preparation modes, several groups have succeeded in forming patterns with gold and silver nanosized particles [17–23].

The single electron tunneling effect on nanometer-sized metals has been recognized to be the fundamental concept for ultimate miniaturization in microelectronics [24]. Considerable progress has been achieved using scanning tunneling microscopy (STM), which constitutes an indispensable tool to explore down to the atomic level. This is primarily based on the ability to image and locally probe the light generated by a biased STM tip from different surfaces. With this, local information on chemical [25,26], electronic [26,27] and optical properties [28,29] can be obtained.

In this paper we describe optical collective properties of silver nanoparticles organized in 2D superlattices. Our aim is to show that we can control optical properties of these particles by controlling the organization state on the substrate. By using the STM-induced photon emission, local optical mode excitations and relaxation mechanisms are examined.

MODELING AND CALCULATION OF THE OPTICAL SPECTRA OF SILVER NANOPARTICLES

In this section we consider silver nanoparticles coated with dodecanethiol. They are either dispersed in a solvent such as hexane and considered as isolated particles or organized on a graphite substrate in a 2D hexagonal network. We calculate the optical properties of these particles either dispersed in a solvent or organized on a substrate.

The absorption spectrum of isolated spherical particles is characterized by the well-known Mie resonance [30–32], occurring at a frequency ω_o such that

$$\varepsilon_{1s}(\omega_o) = -2\,\varepsilon_m$$

where $\varepsilon_s(\omega) = \varepsilon_{1s}(\omega) + i\varepsilon_{2s}(\omega)$ is the dielectric function of the silver spherical particles and ε_m is the dielectric function of the surrounding medium. Because the particles are coated by the dodecanethiol and are dispersed in hexane, the dielectric constant can be assumed to be $\varepsilon_m = 2$. In fact, the dielectric constants of dodecane and hexane solvent are 1.98 and 1.88, respectively. The full half-width of the resonance peak is determined by the imaginary part and also by the slope of the real part of the dielectric function at the frequency ω_1. For randomly oriented ellipsoidal particles, the optical response can be interpreted in terms of the depolarization factors. The optical spectrum is characterized by two resonance peaks corresponding to the polarizabilities along the major and the minor axes [33–39].

The optical spectra of isolated spherical particles coated by an alkyl chain (dodecanethiol) deposited on a substrate with a rather small distance of closest approach are investigated. The optical absorption spectra are deduced from numerical calculations of the extinction cross-section, σ, for clusters of silver spheres by using the calculations described in the literature [40–44]. The dielectric function of the spheres is local and homogeneous and is taken from a Drude-like model which includes a contribution due to the d-electrons. In the calculation, the Maxwell equations are solved by using the convenient boundary conditions at the surface of all the spheres, in the general framework of the method developed by Gerardy and Ausloos. The calculation details are described in [45].

In order to use the calculations performed for finite-size clusters for the description of actual infinite 2D systems, we must make allowance for both the shape and size effects on the results of the
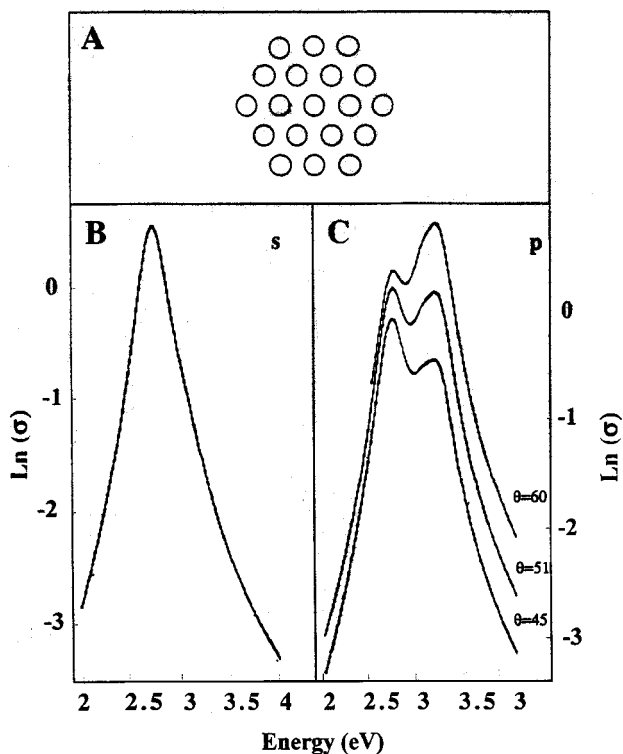
Fig. 1 A) cluster used in the calculation corresponding to the hexagonal structure; B) extinction cross-section for s-polarization; C) p-polarization.

calculations. The clusters that we considered are mainly 19 hexagonally organized particles with 5.3 nm diameter and 1.85 nm spacing between particles (Fig. 1A).

The main features of the spectra are first that there are two resonances at frequencies ω^- and ω^+ with $\omega^- < \omega_o < \omega^+$ and second that the s-polarization spectrum has only a single peak at $\omega = \omega^-$ (Fig. 1B) while the p-polarization spectrum shows both peaks (Fig. 1C), and the amplitude of the high-energy peak increases with the angle of incidence. Such behavior is clearly the result of the optical anisotropy of the system, namely its polarizability has different values in the direction normal to the surface, and in a direction parallel to the surface (for the considered lattice, the system is isotropic in the surface plane). This anisotropy exhibits in the p-polarization case since the incident electric field has a component parallel, E_x, and a component normal, E_z, to the surface, while in the s-polarization case the electric field has only a component parallel to the surface, E_y.

COLLOIDAL SELF-ASSEMBLIES USED AS TEMPLATES

To synthesize colloidal metal dispersions, reverse micelles are used as templates [1].

Reverse micelles are well known to be spherical water in oil droplets stabilized by a monolayer of surfactant. The phase diagram of the surfactant sodium bis(2-ethylhexyl) sulfosuccinate, called Na(AOT), with water and isooctane shows a very large domain of water in oil droplets, and is, therefore, the surfactant most often used to form reverse micelles [1,46]. The water pool diameter is related to the water content, w = [H2O]/[AOT], of the droplet by [1]:

D(nm) = 0.3.w

From the existing domain of water in oil droplets in the phase diagram, the droplet diameters vary from 0.5 nm to 18 nm.

Reverse micelles are dynamic [46,50] and attractive interactions between droplets take place. The intermicellar potential decreases either by decreasing the number of carbon atoms of the bulk solvent or by increasing the number of droplets. This is due to the discrete nature of solvent molecules and is attributed to the appearance of depletion forces between two micelles (the solvent is driven off between the two droplets) [49]. When the droplets are in contact forming a dimer, they exchange their water contents. This exchange process is associated with the interface rigidity, which corresponds to the bending elastic modulus of the interface [50]. Hence, in collisions the droplets exchange their water contents and again form two independent droplets. This process has been used to make metal nanosized particles by chemical reduction of metallic ions [1,3]. We demonstrated that below these various factors (water content, intermicellar potentials) control the particle size.

SYNTHESES OF SILVER NANOPARTICLES DIFFERING BY THEIR SIZES

Syntheses of silver nanosized particles in reverse micelles and control of the size distribution have been described previously [12–13]. Here, colloidal silver particles are prepared by mixing two AOT reverse micellar solutions having the same water content (i.e., molar ratio $W = [H_2O]/[AOT] = 2$). The first contains 30% Ag(AOT) and 70% Na(AOT) and the second hydrazine, N_2H_4, as reducing agent with an overall concentration of 7.10^{-2} M and with 100% Na(AOT). After synthesis, dodecanethiol is added to the micellar solution (1 μl/cm³), and a selective reaction with the silver atoms at the interface of the particles, a monolayer of dodecanethiol, takes place at the silver particles surface. After this process, the average diameter of the particles is 5 nm with 17% size distribution. After syntheses, by varying the amount of dodecanethiol, two procedures are used to control the particles' shape:

1. Immediately after synthesis, the particles are coated with a very small amount of dodecanethiol (0.5 μl/ml) and extracted from micelles and then dispersed in hexane. After 24 hours, the particles flocculate, and those left on the bottom of the vessel are deposited on the substrate. The TEM pattern shows isolated nanoparticles with 5 nm average size and 17% polydispersity. Some aligned particles are observed on the region of the TEM pattern.
2. Immediately after synthesis, 2 μl/ml of dodecanethiol is added to the reverse micelles, and the coated particles are immediately extracted from these micelles and then dispersed in hexane. A size selection takes place. The average diameter of the spherical particles is 5 nm with a rather low size distribution (17%). The particles are highly stable. As the size distribution is reduced to 17%, deposition of these silver nanoparticles on solid substrates by evaporation of the carrier solvent results in the spontaneous assembly of a 2D structure in a hexagonal network (Fig. 2A). This self-assembly results from a balance between hard-sphere repulsion and van der Waals attraction forces.

OPTICAL PROPERTIES OF NANOCRYSTALS EITHER ISOLATED OR DEPOSITED ON A SUBSTRATE

In the following, the optical properties of silver particles are presented. We chose to separate them into three classes :

i.   Nanocrystals are dispersed in hexane and considered as isolated in a medium.
     A well-defined plasmon peak centered at 2.9 eV characterizes the optical spectrum of particles dispersed in hexane (Fig. 3A). The simulated spectrum (dashed line) indicates that the resonance peak is close to a Lorentzian (Fig. 3A). The misfit observed at high energy is due to the interband transitions (4d-5sp) [51]. Such an optical spectrum has been well described by the quasi-static approximation of the Mie theory [30,31]. The bandwidth increases with decreasing particle size
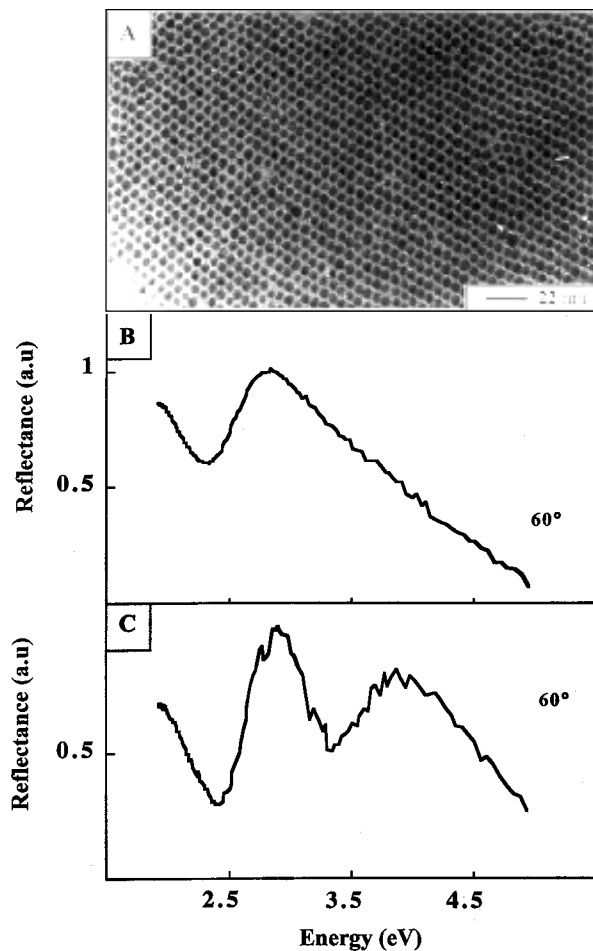
Fig. 2 A) TEM patterns of spherical particles organized on the substrate; B) absorption spectra of silver spherical particles dispersed in hexane; C) reflectance spectra of these particles obtained with p-polarization at 60° incidence angle.

(Fig. 2). This has been well established in these decades [31,40]. It is attributed to a decrease in the electronic mean free path. The calculated spectra show the peak position, ($\omega_o = 2.95$ eV), similar to that obtained from experimental data.

ii. Spherical particles with a very low size distribution, arranged in a hexagonal network on the substrate (Fig. 2A).

The optical spectra of spherical particles organized in 2D superlattices on a graphite substrate show one resonance peak positioned at 2.7 eV [53] under nonpolarized light (Fig. 4). The optical spectrum is shifted toward low energy compared to that of spherical particles dispersed in hexane (2.9 eV). Conversely to what is observed for isolated particles (Fig. 3A), the optical spectra are asymmetrical. For 4-nm silver nanocrystals, an increase in the band width to 1 eV compared to isolated spherical particles (0.7 eV) is observed (Fig. 4). On washing the substrate, the absorption spectra of dispersed particles in hexane is similar to that observed for isolated spherical particles. This indicates that the coated particles do not coalesce after deposition. The observed lack of symmetry can be attributed to additional resonance when particles are organized in a hexagonal network. To investigate the optical anisotropy manifested in terms of the observed asymmetrical band shape, the optical spectra under polarized light are measured.
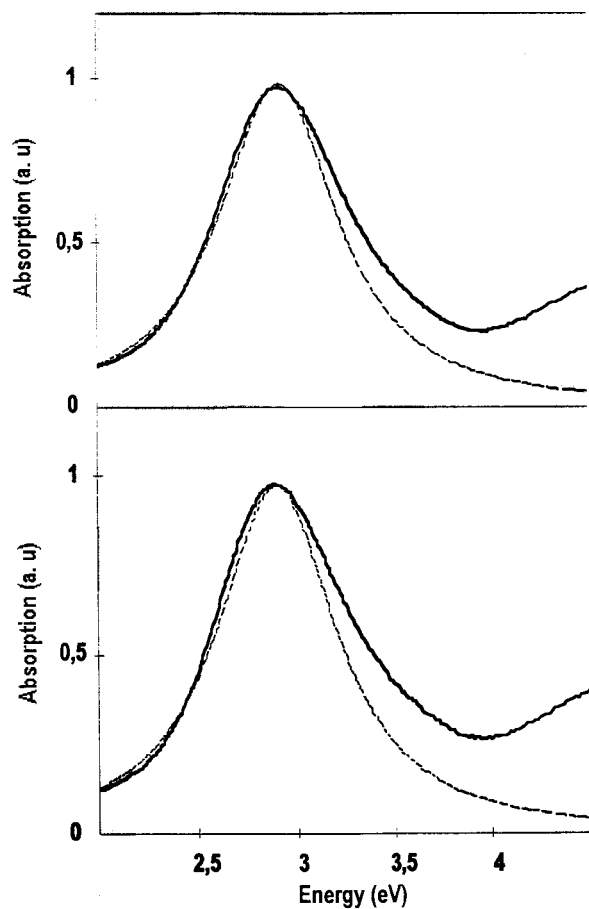
Fig. 3 Absorption spectra, normalized to unity, of silver nanocrystals dispersed in hexane having an average size of 4-nm (A) and 5-nm (B) particles dispersed in hexane normalized to unity.
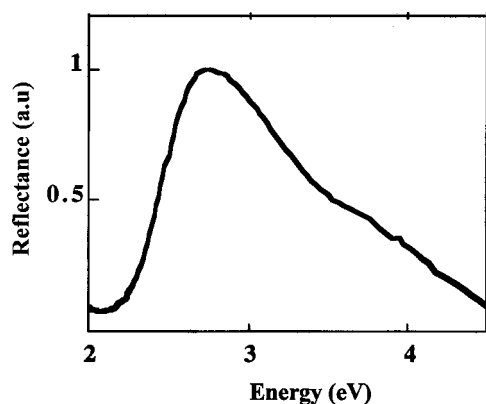

Fig. 4 Reflectance spectra of 5-nm nanocrystals deposited on the substrate under nonpolarized light.

Under s-polarized light, the optical spectra of organized spherical particles, recorded at various incident angles, do not show any change with increasing θ. They are characterized by a resonance at 2.9 eV, which is similar to that observed for isolated particles. However, the plasmon band remains asymmetric as observed under nonpolarized light (Fig. 2B).

Under p-polarization, the optical spectra markedly change with the incident angle. At high θ values (θ = 60°), a new plasmon resonance peak appears at high energy (Fig. 2C). The two
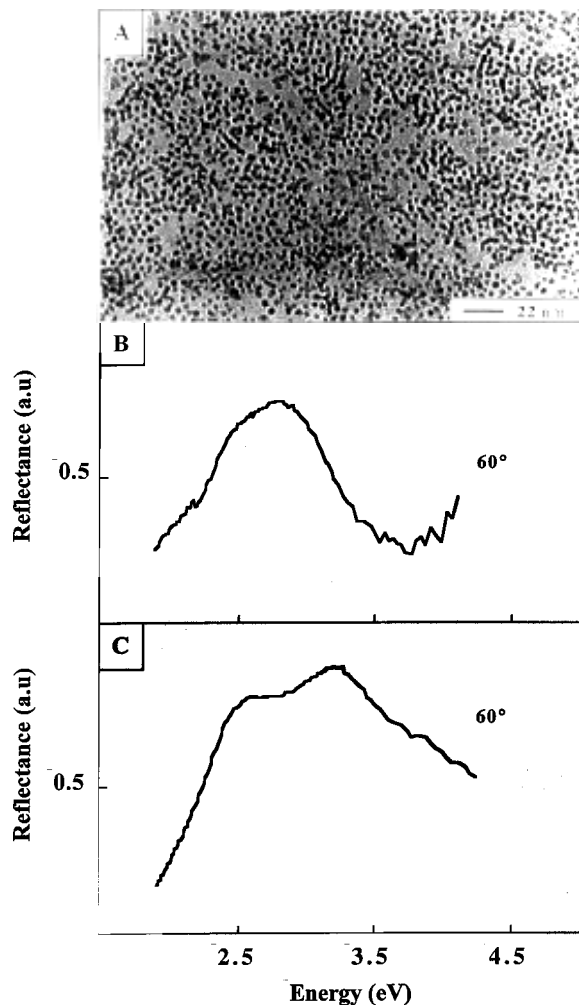
Fig. 5 A) TEM patterns of disordered and coalesced particles on the substrate; B) absorption spectra of these particles dispersed in hexane; C) reflectance spectra of these particles obtained with p-polarization at 60° incidence angle.

observed peaks are well defined: One is centered at 2.8 eV (ω^-) [close to that observed for isolated particles, ($\omega_0 = 2.9$ eV)] whereas the other is centered at 3.8 eV, (ω^+). Hence, when particles are organized in a hexagonal superlattice with 1.8 nm average distance between particles, a new resonance peak appears at high energy whereas the one ($\omega^- = 2.8$ eV) close to that of isolated spherical particles ($\omega_0 = 2.9$ eV) still remains.

iii. Disordered particles on the substrate with mainly spherical particles, some of them are close together or coalesced as shown by the arrow in Fig. 5A.

To investigate the optical properties of disordered or aligned particles randomly deposited on a graphite substrate, reflective polarized light experiments were made at various angles θ.

Under perpendicular polarization to the plane of incidence (s-polarization), the electric-field vector is always directed along the major axis of the spherical particles (parallel to the substrate). This tends to be insensitive to the plasmon mode oriented perpendicular to the substrate [52] and does not provide any information on the optical surface anisotropy. The optical experimental spectra (Fig. 5B) show one resonance at 2.7 eV. This is attributed to the longitudinal plasmon mode parallel to the substrate.

Conversely, under parallel polarization to the plane of incidence field (p-polarization), the electric field has two components: one is along the minor axis corresponding to transversal modes (Fig. 5C). The other is along the major axis corresponding to longitudinal modes. Hence the p-polarization provides information on the optical film anisotropy. The obtained optical response shows a splitting of the spectra at high values of θ, the first peak is shifted toward high energy compared to that of isolated spherical particles, whereas the second is at lower energy. This optical anisotropy, in terms of two resonance peaks, is due to the asymmetrical shape of coalesced particles [36,37].

The comparison between the optical properties of particles deposited on the same substrate [cleaved graphite] and differing by their organizations [spherical organized and disordered particles] led us to the conclusion that the appearance of the resonance peak at 3.8 eV is due to the self-organization of the particles in a hexagonal network. This can be interpreted in terms of mutual interactions between particles. The local electric field results from dipolar interactions induced by particles at a given distance from each other. Near the particles, the field consists of the applied field plus a contribution due to all other dipoles and their images. The calculation performed for finite-size clusters gives, at a qualitative level, a correct explanation of the appearance under s-polarization of one resonance peak and an additional peak toward high energy under p-polarization. For isolated spherical particles, a good correlation of the resonance frequency, between calculation ($\omega_0 = 2.95$ eV) and experimental ($\omega_0 = 2.9$ eV) data is obtained. Conversely, for organized spherical particles, some discrepancies between the experimental and the calculated data are observed. The calculated resonance positions are underestimated in comparison to the experimental value. For example, the absolute value of the low-energy resonance peak, ω^-, is 0.3 eV lower than that determined from the experiments ($\omega^- = 2.8$ eV).

These discrepancies between the experimental data and the calculation may be due to:

a.   the fact that the particles, in first approximation, are assumed to be spherical. In fact, it has been demonstrated that the silver nanocrystals are faceted [21]. This could enhance the optical anisotropy.

b.   We did not take into account the substrate effect. Although, for spherical particles, we do not expect a large change in the shift ($\omega^+ - \omega^-$) due to the substrate [39,53]. The dielectric discontinuity due to the substrate leads to a shift in the resonance peak frequencies [37,39,53]. On the other hand, the substrate may introduce additional changes in the position of the frequencies through specific interactions with the particles and/or the chains of the molecules coating the particles.

We do not invoke either the interband transition or the bulk plasmon resonance in order to explain the high-energy peak observed at 3.8 eV for organized spherical particles. These two effects are characteristic of the bulk material and therefore should depend neither on the state of polarization nor on the shape of the particle. The calculation of the plasmon resonance of small metal particles including the bulk plasmon resonance has been performed by Ruppin, and this resonance leads to a very small amplitude peak which does not depend on the direction of the incident field [43].

LOCAL PHOTON EMISSION OF SELF-ASSEMBLED METAL

Organized arrays of dodecanethiol-capped silver nanoparticles are formed by evaporating the solvent on a Au(111) substrate [54] at room temperature. Figure 6A shows the STM image [55] of close-packed 2D nanoparticles lattices in hexagonal symmetry with 6 nm mean distance between particles (distance center to center). This lattice constant is consistent with 4-nm-diameter silver nanoparticles, separated by a 2-nm gap formed by dodecanethiol chains. These ordered monolayers over a long range have some holes and rings (Fig. 6A) depending on the colloidal solution concentration and the substrate interaction.
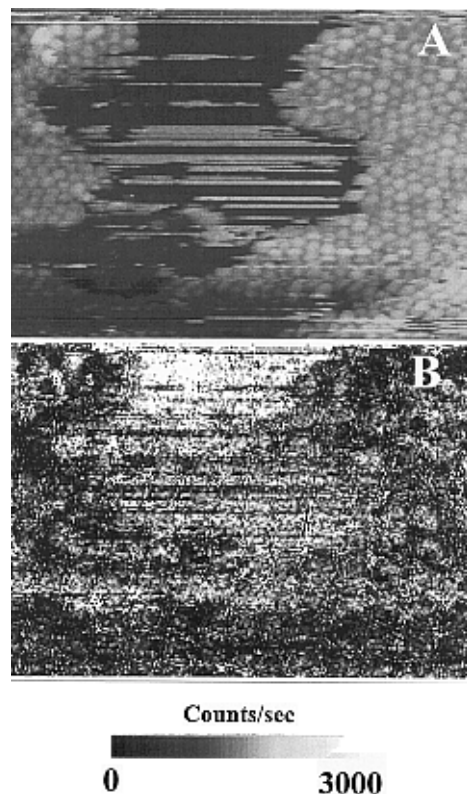
Counts/sec

0   3000

Fig. 6 A) STM image of 5-nm silver nanocrystals self-assembled on a gold substrate and B) the corresponding photon map. Scan area 205×147 nm, sample bias $Vs = 2.5$ V, $It = 1.8$ nA, light intensity ranges from zero (black) to 3 100 counts per second (white). The acquisition time is 1.3 ms per pixel.

From the STM image we observe some horizontal bands (Fig. 6A), explained by the particle motion. In fact, the particles at the border of the uncovered region in the monolayer can drift, under the interaction with the scanning tip. This demonstrates the weak bonding of the particles when they are not fixed inside the network.

The photon emission map shows that both the organized monolayer of nanoparticles and the substrate emit photons when excited by the biased STM tip (Fig. 6B). The intensity of light emission from the Au(111) substrate exceeds that of nanoparticle monolayers by one order of magnitude, reflecting the dependence of plasmon excitation efficiency and radiative relaxation on the material. The gold substrate shows homogenous photon emission. This results in radiative decay of plasmon localized between the STM tip and flat surface. The surprising result is that observed from an ordered nanoparticle monolayer, which manifests inhomogeneous photon emission intensity. A closer analysis of the STM image and photon map over an area of 26×26 nm^2 (Figs. 7A and 7B) shows clearly this photon emission inhomogeneity. Comparison between these two experiments indicates that the dark area coincides exactly with the contour of the particle (Fig. 7B). The light intensity at this dark site (80 cps) decreases by nearly a factor of 10 compared with other neighbors' emission sites.

To correlate the quenching sites (non-emissive) with other phenomena, the STM image obtained for the two fast scan directions (Figs. 8A and 8B) was analyzed. Superimposition of these two images shows that only one particle position has a significant fluctuation amplitude of about 9 Å (Fig. 8C). From the STM image, we note that the diameter of this mobile particle is smaller than that of its neighbors. As other similar smaller particles emit normally, the photon-emission quenching is correlated to the particle motion and not to the particle size.
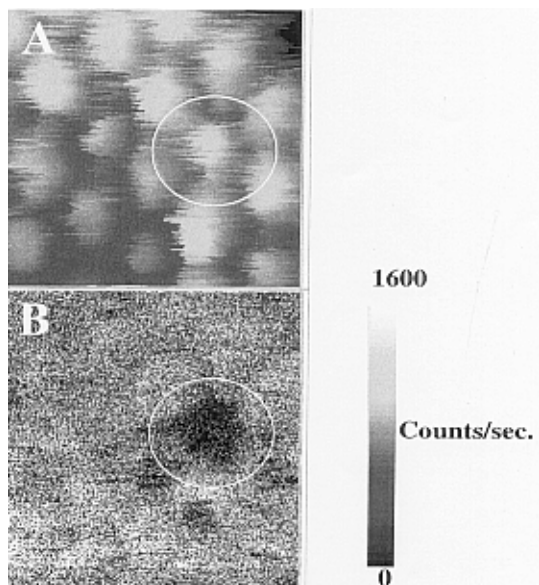
Fig. 7 A) High-resolution STM image of 5-nm silver nanocrystals self-assembled; B) corresponding photon map. Scan area 26 × 24 nm, sample bias Vs = 2.5 V, It = 1.8 nA, light intensity ranges from zero (black) to 1 600 counts per second (white). Arrow indicates fast scan direction. The acquisition time is 2.6 ms per pixel.

The photon maps are recorded by STM in the constant current mode where the total injected current is kept constant throughout the measurement. The prevailing contributions to this current are due to elastic tunneling electrons; the inelastic contribution and the photon emission are therefore free to fluctuate. STM-induced photon emission from metal substrates has been identified as a result of radiative decay of the plasmon mode [3,15,16,25,56,57] excited through inelastic electron tunneling (IET) from the biased tip to the surface [56,57]. A variety of electronic and geometric factors can affect the photon emission intensity on a local scale. Geometric factors such as the tip-sample distance, the characteristic tip radius, and the sample curvature determine the local mode [58,59]. The observed homogeneous photon emission from Au(111) flat terrace substrate is consistent with the previous geo-
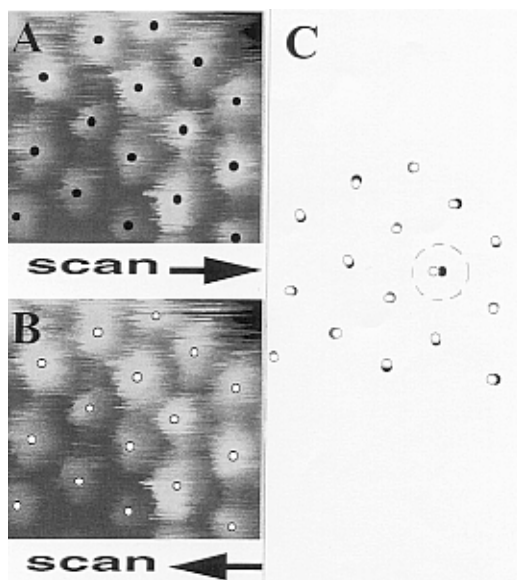

Fig. 8 A and B correspond to the opposite scan directions forward and backward, indicated by arrows. C) Superposition of nanoparticles reveals that only one particle fluctuates notably (about 9 Å). This movable position corresponds to the site of light-emission quenching.

metric factor. In the case of silver nanoparticles, the radius dependence of photon emission contrast could not explain the high intensity variation, as the nanoparticles have a narrow size distribution. Moreover, such a correlation does not appear from the comparison of morphology and photon maps [13].

Electronic properties describe electron relaxation by determining the initial and final density of states available for inelastic processes and will thus modify the branching ratio between elastic and inelastic electron tunneling and hence the photon emission.

The electron can relax to the ground state (the Fermi level), by the plasmon excitation and photon emission or by coupling with the surface phonon modes. As the narrow size distribution of the particles with the mean diameter smaller than the electron mean free path in bulk silver, $\lambda_{MFP} \approx 10$ nm [60], we have ballistic electron transport inside the particles. The electron can relax to the ground state (Fermi level) only by interaction with surface plasmon modes or by coupling with the phonon modes.

It is recognized that with nanoparticles smaller than the bulk mean free path, the phonon modes play an important role in the electron relaxation process [61,62]. As the particles are coated by an insulating layer of dodecanethiol, the applied bias is divided between two barriers, the first between the STM tip and nanoparticle, and the second between nanoparticles and the Au(111) substrate.

Only elastic electron tunneling with excess energy greater than the resonance plasmon energy can excite the local plasmon modes. If the electron scatters by interaction with the surface phonon mode, its excess energy is insufficient to create local plasmon modes, leading to light-emission quenching.

To correlate motion of the particles within their site in the organization with light-emission quenching, we expect significant coupling of the electron with the surface phonon mode for the less-well-bonded particles. This can be explained as the collective phonon mode over several particles for nearly bonded particles, whereas less-well-bonded particles are weakly coupled to phonon modes with neighboring particles.

Further investigations are needed to clarify the electron relaxation process by coupling with the particle phonon mode, or the possible contribution of the electrical coupling with the substrate.

CONCLUSION

Surprisingly, optical anisotropy is observed for organized spherical silver particles on a graphite substrate. A high-energy resonance peak appears under p-polarization and is attributed to the collective effect in terms of mutual interaction between particles. This high-energy peak disappears when particles are either disordered or coalesced. The calculations taking into account interactions between particles provide a qualitative explanation of such behavior. However, the particle–substrate interaction cannot be excluded.

We present results on the local electronic properties of silver nanocrystals. We show, for the first time, the site-dependent quenching photon emission within an organized monolayer of silver nanoparticles. This site-quenching photon emission was correlated to less-bonded particles and explained in terms of electron–phonon coupling enhancement.

ACKNOWLEDGMENTS

REFERENCES

1. M. P. Pileni. *J. Phys. Chem.* **97**, 6961 (1993).
2. J. Fendler and F. C. Meldrum. *Adv. Mater.* **7**, 607 (1995).

3.   M. P. Pileni. *Langmuir* **13**, 3266 (1997).
4.   K. Solecka-Cermakova and B. Vlckova. *J. Phys. Chem.* **100**, 4954 (1996).
5.   A. Badia, W. Gao, S. Singh, L. Demers, L. Cuccia, L. Reven. *Langmuir* **12**, 1262 (1996).
6.   M. Brust, D. Bethell, D. J. Schiffrin, C. J. Kiely. *Adv. Mater.* **7**, 795 (1995).
7.   J. P. Spatz, A. Roescher, M. Moller. *Adv. Mater.* **8**, 337 (1996).
8.   N. Kimizuka and T. Kunitake. *Adv. Mater.* **8**, 89 (1996).
9.   A. S. Tse, Z. Wu, S. A. Asher. *Macromolecules* **28**, 6533 (1996).
10.   S. A. Asher, J. Holtz, L. Liu, Z. Wu. *J. Am. Chem. Soc.* **116**, 4997 (1994).
11.   S. Y. Chang, L. Liu, S. A. Asher. *J. Am. Chem. Soc.* **116**, 6739 (1994).
12.   C. Petit, P. Lixon, M. P. Pileni. *J. Phys. Chem.* **97**, 12974 (1993).
13.   A. Taleb, C. Petit, M. P. Pileni. *Chem. Mater.* **9**, 950 (1997).
14.   L. Motte, F. Billoudet, M. P. Pileni. *J. Phys. Chem.* **99**, 16425 (1995).
15.   L. Motte, F. Billoudet, E. Lacaze, M. P. Pileni. *Adv. Mater.* **8**, 1018 (1996).
16.   L. Motte, F. Billoudet, E. Lacaze, J. Douin, M. P. Pileni. *J. Phys. Chem.* **101**, 138 (1997).
17.   R. L. Whetten, J. T. Khoury, M. M. Alvarez, S. Murthy, I. Vezmar, Z. L. Wang, C. C. Cleveland, W. D. Luedtke, U. Landman. *Adv. Mater.* **8**, 429 (1996).
18.   M. Brust, D. Bethell, D. J. Schiffrin, C. J. Kiely. *Adv. Mater.* **7**, 9071 (1995).
19.   S. A. Harfenist, Z. L. Wang, M. M. Alvarez, I. Vezmar, R. L. Whetten. *J. Phys. Chem.* **100**, 13904 (1996).
20.   J. R. Heath, C. M. Khobler, D. J. Leff. *Phys. Chem. B* **101**, 189 (1997).
21.   S. A. Harfenist, Z. L. Wang, R. L. Whetten, I. Vezmar, M. M. Alvarez. *Adv. Mater.* **9**, 817 (1997).
22.   P. C. Ohara, J. R. Heath, W. M. Gelbart. *Angew. Chem. Int. Ed. Eng.* **36**, (1997) 1077.
23.   W. D Luedthe and U. Landman. *J. Phys. Chem.* **32**, 13323 (1996).
24.   G. Shön and U. Simon. *Colloid Polym. Sci.* **273**, 202 (1995).
25.   R. Berndt and J. K. Gimzewski. *Phys. Rev. B* **48**, 4746 (1993).
26.   R. Berndt, et al. *Science* **262**, 1425 (1993).
27.   C. Thirstrup, M. Sakurai, K. Stokbro, M. Aono. *Phys. Rev. Lett.* **82**, 1241 (1999).
28.   K. Ito, S. Ohyama, Y. Uehara, S. Ushioda. *Surf. Sci.* **324**, 282 (1995).
29.   Ph. Dumas, C. Syrykh, I. V. Makarenko, F. Salvan. *Europhys. Lett.* **40**, 447 (1997).
30.   G. Mie. *Ann. Phys.* **25**, 377 (1908).
31.   C. F. Bohren and D. R. Huffman, eds. *Absorption and Scattering of Light by Small Particles*, Wiley, New York (1983).
32.   S. Yoshida, T. Yamaguchi, A. Kinbara. *J. Opt. Soc. Am.* **61**, 62 (1971), **61,** 463 (1971).
33.   R. Chauvaux and A. Meessen. *Thin Solid Films* **62**, 125 (1979).
34.   P. A. Bobbert and J. Vlieger. *Physica A* **147**, 115 (1987).
35.   M. M. Wind, P. A. Bobbert, J. Vlieger, D. Bedeaux. *Physica A* **157**, 269 (1989).
36.   P. Royer, J. L. Bijeon, J. P. Goudonnet, T. Inagaki, E. T. Arakawa. *Surf. Sci.* **217**, 384 (1989).
37.   P. Royer, J. P. Goudonnet, R. J. Warmack, T. L. Ferrell. *Phys. Rev. B* **35**, 3753 (1987).
38.   R. Ruppin. *Surf. Sci.* **127**, 108 (1983).
39.   R. G. Barrera, M. del Castillo-Mussot, G. Monsivais, P. Villaseñor, W. L. Mochan. *Phys. Rev. B* **43**, 13819 (1991).
40.   U. Kreibig and M. Vollmer. In *Optical Properties of Metal Clusters* (J. Peter Toennies, ed.), Springer Series in Materiel Science 25 (1993).
41.   U. Kreibig and L. Genzel. *Surf. Sci.* **156**, 678 (1985).

42. M. Quinten and U. Kreigig. *Appl. Opt.* **32**, 6173 (1993).
43. R. Ruppin. *Phys. Rev. B* **11**, 2871 (1975).
44. J. M. Gérardy and M. Ausloos. *Phys. Rev. B* **25**, 4204 (1982).
45. A. Taleb, V. Russier, A. Courty, M. P. Pileni. *Phys. Rev. B* **59**, 13350 (1999).
46. "Reactivity in Reverse Micelles" M. P. Pileni, ed. Pub. Elsevier (1989).
47. T. F. Towey, A. Khan-Lodl, B. H. J. Robinson. *J. Chem. Soc. Faraday Trans. 2* **86**, 3757 (1990).
48. C. Robertus, J. G. H. Joosten, Y. K. Levine, *J. Chem. Phys.* **93**, 10, 7293 (1990).
49. G. Cassin, J. P. Badiali, M. P. Pileni. *J. Phys. Chem.* **99**, 12941 (1995).
50. T. K. Jain, G. Cassin, J. P. Badiali, M. P. Pileni. *Langmuir* **12**, 2408 (1996).
51. T. Yamaguchi, M. Ogawa, H. Takahshi, N. Saito, E. Anno. *Surf. Sci.* **129**, 232 (1983).
52. a) S. W. Kennerly, J. W. Little, R. J. Warmack, T. L. Ferrell. *Phys. Rev. B* **29**, 2926 (1984).
    b) D. Blaudez, T. Buffeteau, B. Desbat, P. Fournier, A. M. Ritcey, M. Pezolet. *J. Phys. Chem.* **102**, 99 (1998).
53. A. Taleb, C. Petit, M. P Pileni. *J. Phys. Chem. B* **102**, 2214 (1998).
54. Au(111) films, typically 100 nm thick, are prepared on a mica substrate. Surfaces are further prepared by Argon-ion bombardment and annealing in ultra-high vacuum (UHV) with a base pressure in the low 10^{-10} mbar range. STM-scans of the Au(111) film show that they contain atomically flat, typically 200 nm wide, terraces. A self-assembled nanoparticles monolayer is prepared by placing a drop of freshly prepared solution of silver nanoparticles on the Au(111) substrate. The sample is introduced into a multichamber UHV-STM immediately after evaporation of the silver nanoparticles solution deposited on the substrate.
55. The STM is based on a commercial UHV-STM (Omicron). The STM is housed in a multichamber UHV system, which includes a sample/tip insertion preparation chamber, and the STM chamber, which operates at a base pressure in the low 10^{-10} mbar range. The STM tips are prepared electrochemically using Au wires (0.25 mm diameter) and cleaned after by Argon-ion bombardment. For the photon emission experiments a photon-collection system is adapted to the UHV-STM—a spherical optical system was used to focus light from the tip region to a detector—an avalanche-photodiode photon-counting system (EGG, SPCM-AQ-15, with 35 cps dark count) outside the vacuum system. The spectral range of detection with our system was 400–1000 nm. Our custom-built electronics acquisition system made it possible to obtain simultaneously an STM image and the corresponding photon emission map for both forward and backward directions of the scan. The STM experiments are done in a constant-current mode, and the resolution is 256 pixels per line.
56. R. Berndt, J. K. Gimzewski, P. Johansson. *Phys. Rev. Lett.* **67**, 3796 (1991).
57. P. Johansson, R. Monreal, P. Apell. *Phys. Rev. B* **42**, 9210 (1990).
58. A. Downes, M. E. Taylor, M. E. Welland. *Appl. Phys. Lett.* **72**, 2671 (1998).
59. A. Downes, M. E. Taylor, M. E. Welland. *Phys. Rev. B* **57**, 6706 (1998).
60. C. Girardin. *J. Phys. III France* **6**, 661 (1996).
61. B. A. Smith, J. Z. Zhang, U. Giebel, G. Schmid. *Chem. Phys. Lett.* **270**, 139 (1997).
62. M. Nisoli, et al. *Phys. Rev. Lett.* **78**, 3575 (1997).